References and Notes

1. L. W. Buss, *The Evolution of Individuality* (Princeton Univ. Press, Princeton, NJ, 1987).
2. J. Maynard Smith and E. Szathmáry, *The Major Transitions in Evolution* (Freeman, New York, 1995).
3. D. J. Penn and W. K. Potts, *Am. Nat.* **153**, 145 (1999).
4. M. Carrington *et al.*, *Science* **283**, 1748 (1999).
5. V. Apanius, D. Penn, P. Slev, L. R. Ruff, W. K. Potts, *Crit. Rev. Immunol.* **17**, 179 (1997).
6. S. V. Edwards and P. W. Hedrick, *Trends Ecol. Evol.* **13**, 305 (1998).
7. D. Penn and W. K. Potts, *Proc. R. Soc. London Ser. B* **265**, 1299 (1998).
8. C. Wedekind, T. Seebeck, F. Bettens, A. Paepke, *Proc. R. Soc. London Ser. B* **260**, 245 (1995).
9. C. Ober *et al.*, *Am. J. Hum. Genet.* **61**, 497 (1997).
10. F. M. Burnet, *Nature* **232**, 230 (1971).
11. V. L. Scofield, J. M. Schlumpberger, L. A. West, I. L. Weissman, *Nature* **295**, 499 (1982).
12. J. L. Brown and A. Ecklund, *Am. Nat.* **143**, 435 (1994).
13. S. Paterson and J. M. Pemberton, *Proc. R. Soc. London Ser. B* **264**, 1813 (1997).
14. P. W. Hedrick and F. L. Black, *Am. J. Hum. Genet.* **61**, 505 (1997).
15. L. W. Buss, *Trends Ecol. Evol.* **5**, 352 (1990).
16. R. K. Grosberg, *Q. Rev. Biol.* **63**, 377 (1988).
17. H. Oka and H. Watanabe, *Proc. Imp. Acad. Jpn.* **33**, 657 (1957).
18. B. Rinkevich, R. Porat, M. Goren, *Proc. R. Soc. London Ser. B* **259**, 319 (1995).
19. H. Oka, in *Profiles of Japanese Science and Scientists*, M. Yukawa, Ed. (Kodansha, Tokyo, 1970), pp. 195–206.
20. This situation would be similar to gametophytic self-incompatibility (SI) systems of flowering plants. If both male alleles are expressed on the surface of sperm, this would be similar to plant sporophytic SI. The quantitative predictions of these two SI systems would differ depending, for example, on whether the number of shared alleles (one or two) in a system resembling sporophytic SI quantitatively influences gametic compatibility. Nevertheless, the qualitative prediction (more fertilizations for males sharing no alleles with females) would still hold [see D. Charlesworth, *BioEssays* **17**, 31 (1995)].
21. We reared *B. schlosseri* colonies in 500-liter recirculating seawater aquaria at 18°C using previously described protocols (*23*). We determined the allotypes of prospective parents and their offspring by performing serial pairwise compatibility tests on subclones (about five zooids each) isolated from these colonies against sibling or offspring colonies known to be homozygous for alternative allorecognition alleles (*23*). Fusing colonies displayed a characteristic confluence of their blood vascular systems, indicating that they shared at least one allorecognition allele with their fusion partner. The blood vascular systems of rejecting colonies never fused, and after 12 to 24 hours, we often found a distinct necrotic zone demarcating the two subclones.
22. We established three families of full siblings from controlled laboratory matings between colonies collected from the undersides of floating docks in the small-craft harbor at Berkeley, CA. We bred these families from parental colonies that had been previously determined [by allozyme electrophoresis (*40*)] to be heterozygous for two common marker alleles (designated *PGI-1* and *PGI-2*) at the phosphoglucose isomerase locus, a gene unlinked to the allorecognition locus in *B. schlosseri*. We identified offspring from each of these three matings that were either *PGI-1/1* or *PGI-2/2* homozygotes, and then determined [using fusion assays (*21*)] their genotypes at their allorecognition locus. From each family, we chose three sibling colonies for the sperm competition experiments. One of the sibling colonies, which supplied ripe eggs for fertilizations, was either a *PGI-1/1* or *PGI-2/2* homozygote. We fertilized these eggs in vitro (*40*) using sperm from two siblings, one a *PGI-1/1* (or *PGI-2/2*) homozygote syngeneic to the colony supplying the eggs, the other a *PGI-2/2* (or *PGI-1/1*) homozygote allogeneic to the colony supplying the eggs. In each of three replicate trials for each of the mate competition experiments, we added equal volumes (2.5 ml) of a standardized dilution (5×10^7 sperm per milliliter) of sperm from each sperm parent to a dish containing 5 ml of 0.22 μm–filtered seawater and ≈150 ripe ova surgically removed from the egg parent. Ninety minutes later, we transferred 120 to 140 zygotes into clean dishes containing 50 ml of filtered seawater. We held the dishes at 18°C, daily transferring the developing embryos to clean seawater. When the tadpole larvae hatched on day 6 or 7, we froze them individually at −80°C, pending electrophoresis. We then used cellulose acetate gel electrophoresis to assay 100 fully developed larvae from each mating, and assigned paternity to either the sygeneic or allogeneic sperm parent based on the presence of one or the other diagnostic *PGI* marker.
23. A. Sabbadin, *Acta Embryol. Morphol. Exp.* **10**, 205 (1989).
24. O. Mokady and L. W. Buss, *Genetics* **143**, 823 (1996).
25. L. W. Buss, C. S. McFadden, D. R. Keene, *Biol. Bull.* **167**, 139 (1984).
26. R. K. Grosberg, D. R. Levitan, B. B. Cameron, *Evolution* **50**, 2221 (1996).
27. We initiated lab pedigrees from field-collected parental colonies as described (*26*). Compatibility tests between F_1 colonies were conducted as for *Botryllus* with subcloned explants (three to five polyps each) of these progeny. Fusible or rejecting brother-sister pairs were then grown to maturity and mated, and pairs of F_2 offspring were settled in close proximity on glass slides (*26*). We scored the outcomes of interactions between the growing stolons of 33 to 399 pairs from each of 16 matings (8 between fusible sibs; 8 between unfusible sibs) as fusion (anastomosis of the growing stolons of the two colonies) or rejection (production of hyperplastic stolons, followed by tissue necrosis).
28. L. W. Buss and D. R. Green, *Dev. Comp. Immunol.* **9**, 191 (1985).
29. R. K. Grosberg and J. F. Quinn, in *Invertebrate Historecognition*, R. K. Grosberg, D. Hedgecock, K. Nelson, Eds. (Plenum, New York, 1987), pp. 157–167.
30. A. Grafen, *Anim. Behav.* **39**, 42 (1990).
31. A. Sabbadin and B. Zaniolo, *J. Exp. Zool.* **207**, 289 (1979).
32. D. Stoner and I. L. Weissman, *Proc. Natl. Acad. Sci. U.S.A.* **93**, 15254 (1996).
33. D. Stoner, B. Rinkevich, I. L. Weissman, *Proc. Natl. Acad. Sci. U.S.A.* **96**, 9148 (1999).
34. G. J. Velicer, L. Kroos, R. E. Lenski, *Nature* **404**, 598 (2000).
35. D. P. Matton, N. Nass, A. E. Clarke, E. Newbigin, *Proc. Natl. Acad. Sci. U.S.A.* **91**, 1992 (1994).
36. S. R. Palumbi, in *Endless Forms: Species and Speciation*, D. J. Howard and S. H. Berlocher, Eds. (Oxford Univ. Press, Oxford, 1998), pp. 271–278.
37. V. D. Vacquier, *Science* **281**, 1995 (1998).
38. C. S. Cohen, Y. Saito, I. L. Weissman, *Evolution* **52**, 746 (1998).
39. L. Keller and K. G Ross, *Nature* **394**, 573 (1998).
40. R. K. Grosberg, *Evolution* **45**, 130 (1991).

41. We thank B. Cameron and L. Puryear for their contributions and assistance with hydroid culture and breeding; J. Bull and K. Coyne for useful suggestions; and D. Theide for help with some of the analyses. Supported by NSF (USA) and the Natural Sciences and Engineering Research Council (Canada).

22 May 2000; accepted 28 July 2000

How Snapping Shrimp Snap: Through Cavitating Bubbles

Michel Versluis,[1] Barbara Schmitz,[2] Anna von der Heydt,[1,3] Detlef Lohse[1]*

The snapping shrimp (*Alpheus heterochaelis*) produces a loud snapping sound by an extremely rapid closure of its snapper claw. One of the effects of the snapping is to stun or kill prey animals. During the rapid snapper claw closure, a high-velocity water jet is emitted from the claw with a speed exceeding cavitation conditions. Hydrophone measurements in conjunction with time-controlled high-speed imaging of the claw closure demonstrate that the sound is emitted at the cavitation bubble collapse and not on claw closure. A model for the bubble dynamics based on a Rayleigh-Plesset–type equation quantitatively accounts for the time dependence of the bubble radius and for the emitted sound.

The oceans may be deep, but they are not at all quiet (*1*). Sounds in the oceans include those of waves; rain, hail, and snow; and the biological sounds of fish, dolphins, whales, and snapping shrimp. The latter, in particular, produce the dominant level of ambient noise in (sub)tropical shallow waters throughout the world (*2*). These shrimp usually occur in such large numbers that there is a permanent crackling background noise, similar to the sound of burning dry twigs (*3*). The snapping sound can be heard day and night (*4*), with source levels as high as 190 (*5*) to 210 dB (*6*) (peak to peak) referenced to 1 μPa at a distance of 1 m. This severely limits the use of underwater acoustics for active and passive sonar, both in scientific and naval applications. The frequency spectrum of a snap is broad, ranging from tens of hertz to >200 kHz (*5*). The noise of snapping shrimp is therefore also used as a source for creating pictorial images of objects in the ocean through ensonification (*7*).

A snapping shrimp of the species *Alpheus heterochaelis* (~5.5 cm in size) is shown in Fig. 1A. The shrimp produces the snapping

[1]Department of Applied Physics and J. M. Burgers Research Center for Fluid Dynamics, University of Twente, Post Office Box 217, 7500 AE Enschede, Netherlands. [2]Department of Zoology, Technischen Universität München, Lichtenbergstrasse 4, 85747 Garching, Germany. [3]Department of Physics, Philipps-Universität Marburg, Renthof 6, 35032 Marburg, Germany.

*To whom correspondence should be addressed. E-mail: lohse@tn.utwente.nl

sound by an extremely rapid closure of its large snapper claw, which may reach 2.8 cm in length, about half of its body size. The claw (Fig. 1B) has a protruding plunger on the dactyl and a matching socket in the propus. Before snapping, the claw is cocked open by co-contraction of an opener and a closer muscle, building up tension until a second closer muscle contracts (*8*). This results in an extremely rapid closure of the claw (*9*). A high-velocity water jet (*10, 11*) is formed when the dactyl plunger is driven into the propus socket, displacing water. The water jet is received and analyzed by sensory hairs on the snapper claw of conspecific snapping shrimp. Therefore, the snapping plays an important role in intraspecific communication (*12*). In addition, it is used to defend a shelter or territory and to stun and even kill prey animals (*10, 13*).

The loud snap has been attributed to the mechanical contact made when the dactyl and the propus edges hit each other as the claw closes (*6, 14*). Here, we show that the sound originates solely from the collapse of a cavitation bubble that is generated by the fast water jet resulting from the rapid claw closure. The water jet velocity is so high that the corresponding pressure drops below the vapor pressure of water. Seawater contains tiny air bubbles, called nuclei (*15*). Such a microbubble, if located between the dactyl and the propus of the snapper claw, will grow in size when it is entrained in the region of low pressure generated through the water jet. Subsequently, it collapses violently when the pressure rises again.

The experiments were performed with seven individuals of *A. heterochaelis*. Each shrimp was positioned on a small textile platform in a seawater aquarium and tethered to a vertical holder by a plastic nut glued to its back. The snap was evoked by gently touching the freely movable snapper claw with a soft paintbrush. A hydrophone with an upper frequency limit of 100 kHz was positioned at a small distance from the shrimp. Simultaneously, high-speed images were recorded with a digital monochrome video camera at a frame rate of 40,500 frames per second (fps) with a resolution of 64 by 64 pixels. The image acquisition was triggered by the sound of the snap. A typical hydrophone signal is shown in Fig. 2A (*16*). The main peak at time $t = 0$ is followed by a very broadband signal, which is partly due to the reflections of the main signal at the aquarium walls located at a minimum distance of 15 cm. Therefore, the first reflections start after 200 μs. The hydrophone signal shows a precursor signal before the main peak, similar to that previously observed in recordings of the smaller *Synalpheus paraneomeris* snapping shrimp (*5*).

A sequence of high-speed images, showing the snapper claw from the top, is shown in Fig. 2B. The snapper claw is in its cocked position in frame 1. Full closure of the claw is achieved at frame 2 (600 μs later), followed by bubble growth (within 375 μs, although the onset of bubble growth is not visible in this view) and bubble collapse (in <300 μs) at $t = 0$ in frame 3. The images show that the cavitation bubble, which was recorded in each of our 108 experiments, is nonspherical and elongated in the direction of the water jet. The bubble grows to a maximum equivalent radius of 3.5 mm on average. At collapse (frame 3), the transparent single cavitation bubble breaks apart, and an opaque cloud of small bubbles is formed, which finally dissolves.

The temporal correlation between the snapping sound and the bubble dynamics was determined from these high-speed video recordings. The hydrophone signal and the ex-

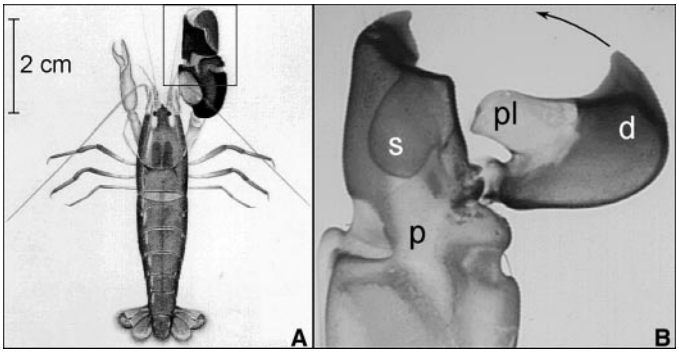

Fig. 1. (**A**) *Alpheus heterochaelis*, one of the largest snapping shrimp. The large snapper claw may be either on the right or the left in both sexes. Modified after (*30*). (**B**) Close-up of the snapper claw in its cocked position. The claw is made transparent by the use of methyl salicylate. The claw has a protruding plunger (pl) on the dactyl (d) and a matching socket (s) in the immobile propus (p) (photograph by B. Seibel). During the extremely rapid closure of the snapper claw, a high-velocity water jet is formed when the plunger displaces the water from the propus socket.

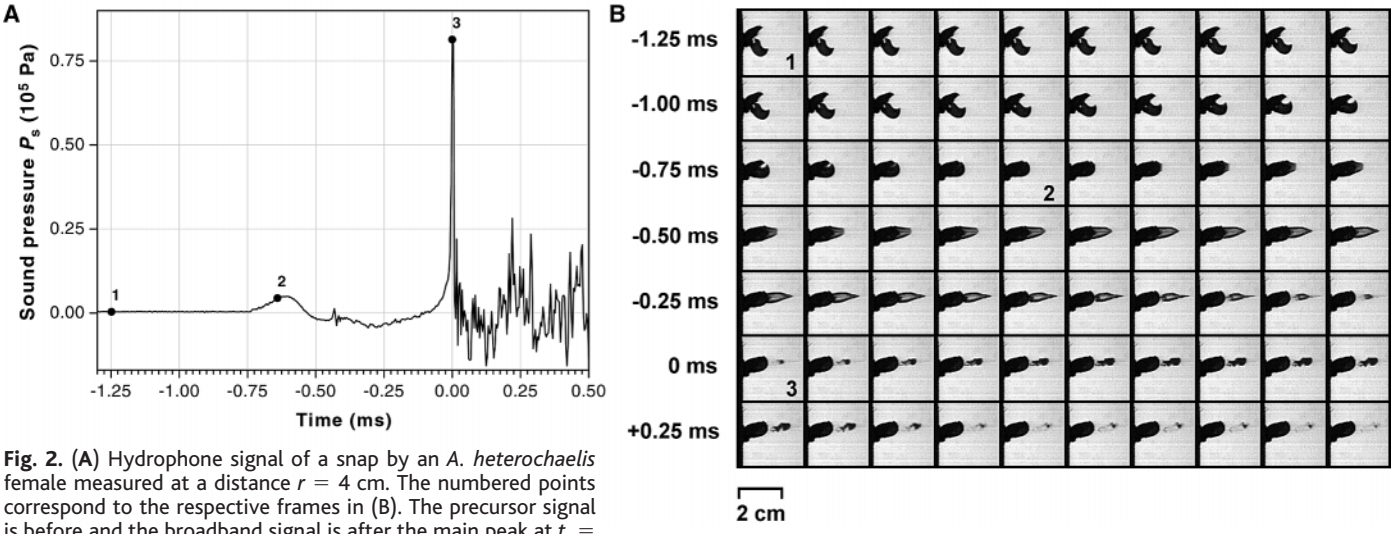

Fig. 2. (**A**) Hydrophone signal of a snap by an *A. heterochaelis* female measured at a distance $r = 4$ cm. The numbered points correspond to the respective frames in (B). The precursor signal is before and the broadband signal is after the main peak at $t = 0$. The broadband signal is partly due to the reflections of the main signal at the aquarium walls. The small peak at $t = -425$ μs coincides with the collapse of a small cavitation bubble under the claw (*29*). (**B**) A sequence of high-speed images in top view showing the closure of the snapper claw taken at 25-μs intervals (40,500 fps). Each tick mark on the time axis of the hydrophone signal (A) indicates an image recording. The dactyl rotation starts at frame 1 at $t = -1250$ μs. The main peak of the sound emission is at $t = 0$ (frame 3) and coincides with the collapse of the cavitation bubble. Full closure of the claw was already achieved at frame 2, 650 μs before bubble collapse.

posure timing of the high-speed camera were measured simultaneously, referenced to a trigger signal. The main peak of the snapping sound and the collapse of the cavitation bubble always coincide. An analysis of 19 different experiments showed that the temporal correlation of sound and bubble collapse is achieved with a standard deviation of 0.86 frames, i.e., accurate to within 25 μs. The claw is closed in frame 2 of Fig. 2, 650 μs (or 26 frames at 40,500 fps) before bubble collapse.

The angular velocity of dactyl rotation was determined from the position of the tips of the dactyl and propus in relation to the position of the pivot point. Claw closure begins with moderate angular velocities (on the order of 100 rad/s) for large opening angles. In the final stage of claw closure, the dactyl rotates with an impressive 3500 rad/s. Angular velocities of this order were previously measured with a thin laser-coupled optical fiber glued to the distal tip of the dactyl (*9*).

The occurrence of cavitation bubbles explains why the snaps are harmful to prey animals: It is cavitation damage, known to damage ship propellers and centrifugal pumps. The destructive force of a collapsing cavitation bubble can be seen during interspecific encounters. Small prey (e.g., worms, goby fish, or other shrimp) can be stunned or killed (*13*), and small crabs (*Eurypanopeus depressus*) are injured by the snap of snapping shrimp (*17*). The interaction distance, defined as the distance from the tip of the snapper claw to the nearest body part of the opponent measured along the long axis of the snapper claw, was reported to be 3 mm on average. In our experiments, it is shown that the cavitation bubble collapses 3 mm in front of the tip of the snapper claw (Fig. 2). In intraspecific encounters, the snap does not injure the opponent; the interaction distance is 9 mm on average (*12*), far enough to avoid implosion danger.

The velocity of the water jet was estimated from the speed of the cavitation bubble. High-speed video close-ups of the cavitation bubble indicate velocities of the front end of the bubble as high as 32 m/s, whereas the bubble expands longitudinally with a speed of 9 m/s. This indicates a flow with a speed v_{max} on the order of 25 m/s. This high water jet velocity implies a pressure drop from the ambient pressure $P_0 = 10^5$ Pa, which can, in principle, be modeled through Bernoulli's law. However, there is limited information on the actual temporal and spatial shape of the velocity field and, consequently, also on the pressure field. Nevertheless, the unsteady term in Bernoulli's law, $\rho\partial_t\phi$ (where ρ represents the density of water, ∂_t is the partial derivative with respect to time, and ϕ is the velocity potential), can be estimated by dimensional arguments and is smaller than or, at most, of the same order of magnitude as the kinetic energy term. Therefore, we estimate the magnitude of the pressure drop as $P_a \sim (1/2)\rho v_{max}^2$. With the above water jet velocity, $P_a \sim 3 \times 10^5$ Pa. Moreover, we assume a Gaussian pressure distribution in time

$$P(t) = P_0 - P_a \exp\left[-4 \ln 2 \frac{(t - t_0)^2}{\sigma^2}\right] \quad (1)$$

where σ represents the width of the Gaussian pulse. As the pressure $P(t)$ drops below the vapor pressure of water ($P_{vap} = 2 \times 10^3$ Pa), cavitation occurs.

The bubble that arises at the tip of the snapper claw is not spherical. Modeling the dynamics of nonspherical bubbles is nontrivial (*18*), requiring that all parameters, such as the water jet velocity and width and the size and shape of the bubble nucleus, be precisely known. However, to get at least a semiquantitative statement, we can assume a spherical bubble, whose dynamics is well described by Rayleigh-Plesset–type equations (*15*).

Typical bubble nuclei in seawater are between 1 and 50 μm in radius (*15, 19*). We assume a nucleus initially filled with air and of the initial radius $R_0 = 10$ μm under normal conditions. The results hardly depend on the choice of R_0. The response of the bubble nucleus on the pressure reduction (Eq. 1) is described by the (modified) Keller equation (*20*), which is of Rayleigh-Plesset type

$$\left(1 - \frac{\dot{R}}{c}\right) R\ddot{R} + \frac{3}{2}\left(1 - \frac{\dot{R}}{3c}\right)\dot{R}^2 = -4\nu\frac{\dot{R}}{R} - \frac{2S}{\rho R} + \frac{1}{\rho}\left(1 + \frac{\dot{R}}{c}\right)[p(R, t) + P_{vap} - P(t)] + \frac{R}{\rho c}\frac{d}{dt}p(R, t) \quad (2)$$

The parameters for an air bubble in water are the viscosity of water ν, its density ρ, the speed of sound c, and the surface tension of the air-water system S. The terms proportional to $\dot{R}/c$ take into account the effects of liquid compressibility. $p(R, t)$ is the pressure inside the bubble and can be modeled by a van der Waals equation of state. From an estimation of the Peclét number, we find that we can assume adiabatic behavior (*15, 21, 22*), and because the amount of water vapor inside the bubble is diffusion-controlled (*23*), we couple an additional equation for the water vapor concentration inside the bubble to the Keller equation (*24*). For given bubble dynamics $R(t)$, the emitted sound wave at distance r from the bubble simply follows from (*25, 26*)

$$P_s(r, t) = \frac{\rho R}{r}(2\dot{R}^2 + R\ddot{R}) \quad (3)$$

In Fig. 3, the modeled pressure reduction (Eq. 1) and the calculated bubble radius resulting from Eq. 2 are plotted. As the pressure decreases, the bubble begins to grow up to a maximum radius of ~3.6 mm. There is a time delay through inertia: At maximum bubble radius, the pressure has already risen again to the ambient pressure P_0. Subsequently, the bubble collapses rapidly within ~300 μs. After the bubble collapse, the numerical solution of Eq. 2 shows some afterbounces. These are not observed in the experiment, as the bubble is destroyed upon collapse. Indeed, if we perform a linear stability analysis of the spherical bubble (*22, 27*), we find exactly the same feature at bubble collapse: The bubble is destroyed through a Rayleigh-Taylor–type instability.

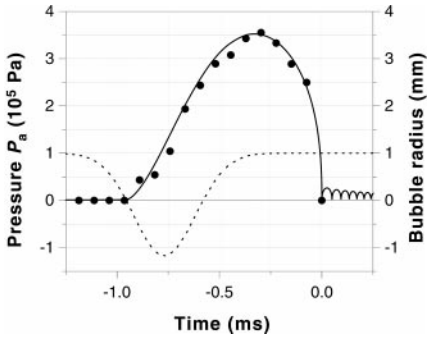

Fig. 3. The calculated bubble radius $R(t)$ as a function of time (solid line). The temporal change of the pressure field $P(t)$ that was modeled for this calculation is also given (dashed line). The model parameters ($P_a = 2.2 \times 10^5$ Pa and $\sigma = 360$ μs) were fitted to match the theoretical radius with the experimentally determined equivalent bubble radius of the ellipsoidal cavitation bubble (indicated by solid circles).

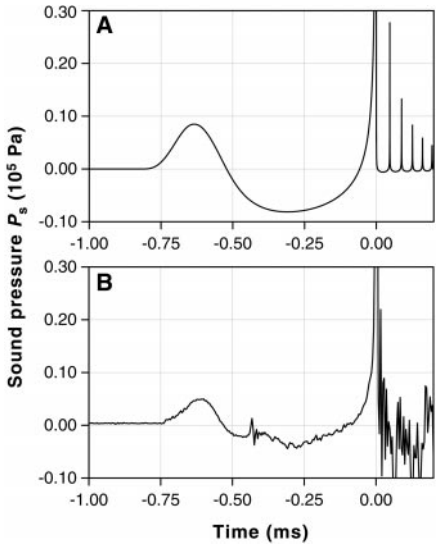

Fig. 4. (**A**) The calculated sound pressure $P_s(r, t)$ for $r = 4$ cm with $P_a = 3.0 \times 10^5$ Pa and $\sigma = 210$ μs. The main peak at $t = 0$ ($P_s = 2 \times 10^8$ Pa) is drawn off-scale to emphasize the precursor signal. (**B**) An enlarged view of the experimental sound pressure curve of Fig. 2.

The model parameters P_a and σ were fitted to match the theoretical radius with the experimentally determined equivalent bubble radius of the ellipsoidal cavitation bubble (solid circles in Fig. 3). With these model parameters, the calculated sound pressure curve (from Eq. 3) is in good agreement with the experimental sound signal (Fig. 4). The main acoustical signal is preceded by a small sinusoidal precursor, caused by the bubble expansion and contraction. At collapse ($t = 0$), the main acoustical signal is emitted. The narrow peaks in the calculated sound signal after the main pressure peak are produced by the aforementioned afterbounces and should not be considered here, as the bubble is destroyed on collapse. Quantitatively, the model overestimates the measured sound pressure, especially the maximum pressure, for three reasons: (i) The nonspherical shape of the real bubble reduces the strength of the collapse and therefore the intensity of the emitted sound, (ii) thermal damping effects (*28*) are not included in the model, and (iii) on the experimental side, the limited bandwidth of the hydrophone underestimates the peak value of the sound pressure.

The calculated width of the main acoustical peak for the modeled spherical bubble is very small, on the order of 100 ps. This δ-like pulse corresponds to a white noise spectrum, consistent with the wide frequency range of the sound of the snapping shrimp. A more quantitative comparison of the theoretical and experimental spectrum must include the asphericity of the collapse, the acoustical emission of the bubble fragments, and the sound reflections from the walls into the model.

The variation in claw size, claw shape, cocking duration, applied closer muscle force, and claw closure speeds of snapping shrimp all lead to slightly different sound signals and have different water jet characteristics. By adjusting the parameters P_a and σ in our model, we are able to account for the variety of precursor signals measured in our experiments (*29*).

References and Notes

1. R. J. Urick, *Principles of Underwater Sound* (McGraw-Hill, New York, 1983).
2. D. H. Cato and M. J. Bell, *Material Research Laboratory Technical Report MRL-TR-91-23* (Defence Science and Technology Organisation, Sydney, Australia, 1992).
3. M. W. Johnson, F. A. Everest, R. W. Young, *Biol. Bull.* **93**, 122 (1947).
4. F. A. Everest, R. W. Young, M. W. Johnson, *J. Acoust. Soc. Am.* **20**, 137 (1948).
5. W. W. L. Au and K. Banks, *J. Acoust. Soc. Am.* **103**, 41 (1998).
6. B. Schmitz, in *The Crustacean Nervous System*, K. Wiese, Ed. (Springer-Verlag, Berlin, in press).
7. C. L. Epifanio, J. R. Potter, G. B. Deane, M. L. Readhead, M. J. Buckingham, *J. Acoust. Soc. Am.* **106**, 3211 (1999).
8. R. E. Ritzmann, *J. Comp. Physiol.* **95**, 217 (1974).
9. B. Schmitz and J. Herberholz, in *New Neuroethology on the Move, Proceedings of the 26th Göttingen Neurobiology Conference 1998*, vol. 2, N. Elsner and R. Wehner, Eds. (Thieme, Stuttgart, 1998), p. 241.
10. J. Herberholz and B. Schmitz, *J. Comp. Physiol. A* **185**, 41 (1999).
11. H. Schein, *Mar. Behav. Physiol.* **3**, 83 (1975).
12. J. Herberholz and B. Schmitz, *Biol. Bull.* **195**, 156 (1998).
13. G. E. MacGinitie and N. MacGinitie, *Natural History of Marine Animals* (McGraw-Hill, New York, 1949).
14. P. Volz, *Z. Morph. Oekol. Tiere* **34**, 272 (1938).
15. C. E. Brennen, *Cavitation and Bubble Dynamics* (Oxford Univ. Press, New York, 1995).
16. Video files of the snapping shrimp and links to audio files can be found at *Science* Online (available at www.sciencemag.org/feature/data/1052273.shl).
17. S. Schultz, K. Wuppermann, B. Schmitz, *Zool. Anal. Complex Syst.* **101** (suppl. I), 85 (1998).
18. J. R. Blake, Y. Tomita, R. P. Tong, *Appl. Sci. Res.* **58**, 77 (1998).
19. S. L. Ceccio and C. E. Brennen, *J. Fluid Mech.* **233**, 633 (1991).
20. A. Prosperetti and A. Lezzi, *J. Fluid Mech.* **168**, 457 (1986).
21. M. S. Plesset and A. Prosperetti, *Annu. Rev. Fluid Mech.* **9**, 145 (1977).
22. S. Hilgenfeldt, D. Lohse, M. Brenner, *Phys. Fluids* **8**, 2808 (1996).
23. B. D. Storey and A. J. Szeri, *Proc. R. Soc. London Ser. A* **456**, 1685 (2000).
24. R. Tögel, B. Gompf, R. Pecha, D. Lohse, *Phys. Rev. Lett.*, in press.
25. L. D. Landau and E. M. Lifshitz, *Fluid Mechanics* (Pergamon, Oxford, 1987).
26. S. Hilgenfeldt, D. Lohse, M. Zomack, *Eur. Phys. J. B* **4**, 247 (1998).
27. A. Prosperetti, *Q. Appl. Math.* **35**, 339 (1977).
28. Y. Hao and A. Prosperetti, *Phys. Fluids* **11**, 2008 (1999).
29. M. Versluis, B. Schmitz, A. von der Heydt, D. Lohse, in preparation.
30. W. K. Brooks and F. H. Herrick, *Mem. Natl. Acad. Sci. Wash.* **5**, 319 (1891).

31. This work was supported by a grant from the Stichting voor Fundamenteel Onderzoek der Materie (FOM) and by a grant from the Deutsche Forschungsgemeinschaft (Schm 693/5-4) to B.S. The experimental assistance of M. Hansbauer is gratefully acknowledged. We offer special thanks to N. Franz of the electronics workshop of the Department of Physics, Technical University of Munich, for repairing our Schmitt trigger device on Christmas Eve. M.V. is supported by FOM. A.H. is supported by the German-Israeli Foundation.

17 May 2000; accepted 20 July 2000

Detecting and Measuring Cotranslational Protein Degradation in Vivo

Glenn C. Turner and Alexander Varshavsky*

Nascent polypeptides emerging from the ribosome and not yet folded may at least transiently present degradation signals similar to those recognized by the ubiquitin system in misfolded proteins. The ubiquitin sandwich technique was used to detect and measure cotranslational protein degradation in living cells. More than 50 percent of nascent protein molecules bearing an amino-terminal degradation signal can be degraded cotranslationally, never reaching their mature size before their destruction by processive proteolysis. Thus, the folding of nascent proteins, including abnormal ones, may be in kinetic competition with pathways that target these proteins for degradation cotranslationally.

Nascent polypeptides emerging from the ribosome may, in the process of folding, present hydrophobic patches and other structural features that serve as degradation signals similar to those recognized by the ubiquitin (Ub) system in misfolded or otherwise damaged proteins (*1*). Whether a substantial fraction of nascent polypeptides is cotranslationally degraded is a long-standing question.

The Ub sandwich technique was developed to detect cotranslational protein degradation by measuring the steady-state ratio of two reporter proteins whose relative abundance is established cotranslationally. The technique requires that the polypeptide to be examined for cotranslational degradation, termed **B**, be sandwiched between two stable reporter domains, **A** and **C**, in a linear fusion protein (Fig. 1A). The three polypeptides are connected by Ub moieties, creating an **A**Ub-**B**Ub-**C**Ub fusion protein. Ub-specific processing proteases (UBPs) cotranslationally cleave such linear Ub fusions at the C-terminal residue of Ub (*2*–*4*), generating three independent polypeptides, **A**Ub, **B**Ub, and **C**Ub (*5*). UBP-mediated cleavage establishes a kinetic competition between two mutually exclusive events during the synthesis of **A**Ub-**B**Ub-**C**Ub: cotranslational UBP cleavage at the **B**Ub-**C**Ub junction to release the long-lived **C**Ub module or, alternatively, cotranslational degradation of the entire **B**Ub-**C**Ub nascent chain by the proteasome (*6*) (Fig. 1B). In the latter case, the processivity of proteasome-mediated degradation results in the destruction of the Ub moiety between **B** and **C** before it can be recognized by UBPs. The resulting drop in levels of the **C**Ub module relative to levels of **A**Ub, referred to as the C/A ratio, reflects the cotranslational degradation of domain **B** (Fig. 1B).

Division of Biology, California Institute of Technology, Pasadena, CA 91125, USA.

*To whom correspondence should be addressed. E-mail: avarsh@caltech.edu

How Snapping Shrimp Snap: Through Cavitating Bubbles

Michel Versluis, Barbara Schmitz, Anna von der Heydt, and Detlef Lohse

Science, 289 (5487), • DOI: 10.1126/science.289.5487.2114